*remote sensing*

MDPI

*Article*

# A Frequency Selecting Method for High-Frequency Communication Based on Ionospheric Oblique Backscatter Sounding

**Chuqi Cai, Guobin Yang *, Tongxin Liu and Chunhua Jiang**

School of Electronic Information, Wuhan University, Wuhan 430072, China; chuqi_cai@whu.edu.cn (C.C.); tongxin_liu@whu.edu.cn (T.L.); chuajiang@whu.edu.cn (C.J.)
* Correspondence: gbyang@whu.edu.cn; Tel.: +86-27-6877-8049

**Abstract:** Ionospheric oblique backscatter sounding is an effective means of monitoring the ionosphere which can be used as a frequency selection system to serve HF communication and ensure its quality and stability. But how to obtain effective information from the oblique backscatter ionogram is still a hot issue. Due to this situation, a frequency selecting method for HF communication based on ionospheric oblique backscatter sounding is proposed in this study. After obtaining the ionograms, pattern recognition is used to separate the vertical echoes and the oblique backscatter echoes. Next, the leading edge of the oblique backscatter echoes are extracted, and then a two-dimensional electron density profile can be reconstructed. Then, with the help of ray tracing, the usable frequency range can be estimated. Finally, according to the signal-to-noise ratio reflected by the ionograms, several optimal communication frequencies can be selected. In order to verify this method, oblique ionograms are obtained through oblique sounding experiments to evaluate its accuracy. The result indicates that the usable frequency range and the selected frequencies are in accordance with the echo of the oblique ionogram, so the practicability and accuracy of the method are validated. Eventually, the maximum usable frequencies (MUFs) obtained from oblique backscatter sounding are compared with the MUFs from the oblique sounding ionogram; its Mean Absolute Percentage Error (MAPE) is 7.8% and its root mean squared error (RMSE) is 1.34 MHz.

**Keywords:** HF communication; ionospheric oblique backscatter sounding; pattern recognition; ionogram inversion; ray tracing; frequency selecting; max usable frequency

check for updates

**Citation:** Cai, C.; Yang, G.; Liu, T.; Jiang, C. A Frequency Selecting Method for High-Frequency Communication Based on Ionospheric Oblique Backscatter Sounding. *Remote Sens.* **2024**, *16*, 4095. https://doi.org/10.3390/rs16214095

Academic Editor: Yunbin Yuan

Received: 31 August 2024
Revised: 19 October 2024
Accepted: 31 October 2024
Published: 2 November 2024

**Copyright:** © 2024 by the authors. Licensee MDPI, Basel, Switzerland. This article is an open access article distributed under the terms and conditions of the Creative Commons Attribution (CC BY) license (https://creativecommons.org/licenses/by/4.0/).

## 1. Introduction

High-frequency (HF) communication, also called short-wave communication, is one of the most important means of radio communication. Radio waves are transmitted from certain equipment and then reflected by the ionosphere so that they can reach the receiving equipment. HF communication is able to communicate over remote distances and is not constrained by network hubs; in addition, it is also the only means of long-range communication that is not compromised by active mediators [1]. The frequency of HF communication ranges from 3 MHz to 30 MHz; through multiple reflections from the ionosphere, skywaves are able to have global coverage, including reaching some particular areas such as mountains, oceans, and the Gobi Desert that cannot be covered by ultra-short-wave communication [2]. HF communication can operate without the use of satellites, so the construction and maintenance costs are low. It has a number of advantages such as great flexibility, resistance to destruction, and strong stability.

In the past 20 years, the techniques in computer science and communication have flourished, contributing to the rapid upgrading of HF communication technology and equipment [3]. Incorporating digital signal processing, spread-spectrum communication [4], adaptive technology, and other modern information technology, HF communication quality has been substantially improved.

Currently, autonomous frequency selection techniques used in HF communication incorporate spectrum sensing techniques and historical communication data, demonstrating superior performance. However, the disadvantage is that the technique does not take into account ionospheric factors, but only carries out real-time frequency selection based on noise and historical empirical data. Because of the complex local noise environment, the numerous external interferences, and the narrow channel bandwidth, the demand of HF radio and communication systems in terms of situational awareness of the electromagnetic environment and the efficiency and quality of frequency usage is particularly prominent. At the same time, the present autonomous frequency selection techniques do not take into account coordination among users and may face frequency selection conflicts when carrying out regional networking. Especially in small areas, the effect of frequency selection may be reduced, and electromagnetic interference, [5] as well as position exposure and other problems, may be encountered. The ionosphere is a highly dependent channel for HF communication, and its dispersion time-varying nature will lead to an impact on its effect. Since the condition of the ionosphere is greatly affected by solar activity and seasonal changes, and anomalous states [6] occur frequently [7], it is necessary to switch between different communication frequencies on the basis of the conditions to ensure the quality and stability of HF communication. With the development of ionospheric sounding data technology, the introduction of it and environmental monitoring data into autonomous frequency selection can further subserve the accuracy of frequency selection and meet the needs of regional networking.

Ionospheric sounding is mainly about obtaining the parameter characteristics of the ionosphere in a certain region through the form of networking, as well as constructing the ionospheric model using the parameters, ray tracing, and other techniques to realize regional HF frequency planning and channel characteristic assessments [8]. According to the method and process of propagation, ionospheric sounding can be divided into two modes, one is ground-based sounding and the other is sky-based sounding. In ground-based ionospheric sounding, there are vertical sounding, oblique sounding, and oblique backscatter sounding. Among them, vertical sounding is the most classic and widely used sounding method, which transmits signals vertically upwards and receives the echoes at the same location due to the reflection of radio waves by the ionosphere. Vertical sounding can only obtain information of the local ionospheric condition; if we need to obtain ionospheric condition information in a wider region, it is necessary to utilize oblique sounding and oblique backscatter sounding techniques.

Ionospheric oblique backscatter sounding has become an important means of detection because of its wide detection range, real-time detectability, and other advantages. Unlike vertical and oblique ionospheric soundings, which can only acquire ionospheric information for a limited area, the oblique backscatter ionospheric sounding is quite different. In 1927, Eckersley discovered backscattered signals reflected from the ground, bringing the ionospheric oblique backscatter sounding into our view. The signal is transmitted upwards diagonally, reflected by the ionosphere, and finally reaches a distant place; because of the backscattering effect of the ground, part of the signal will return to the transmitting station through the original path and be captured by the receiving equipment [9]. By reason of the wide elevation angle covered by the transmitted wave beam, a large range of ionospheric properties can be obtained in this way, covering even thousands of kilometers, and the results are named as oblique backscatter ionograms. An oblique backscatter ionogram has a very steep echo leading edge on account of the focusing effect of the ionosphere [10]. Extracting the leading edge and performing an inversion of it allows us to obtain the desired ionospheric information.

The use of an ionospheric oblique backscatter ionosonde can provide information on the condition of the ionosphere or the oceans within a radius of several thousand kilometers in an all-round way. Up to now, no other ground-based sounding technology has been able to give such a wide coverage of the ionosphere, land, and oceans; therefore, it is an extremely promising method of detecting the space environment at a long distance. The

use of ionospheric oblique backscatter sounding can detect the ionospheric condition and HF channel characteristics in real time, including the following information [11]:

(1) Information on the structure of the ionosphere along a certain sounding path;

(2) Information on the HF channel characteristics of the ionosphere along the sounding path;

(3) Information on the intensity of the backscattered signal energy;

(4) Information on the propagation patterns of the HF skywave.

The ionosphere has a different influence on HF waves of different frequencies. There are two key frequency values that need to be understood by both sides when establishing a skywave propagation link for communication.

The first one is called the maximum usable frequency (MUF). It is used to describe the highest frequency at which the HF skywave can propagate on a particular path [12,13]. Waves whose frequencies are higher than the MUF will penetrate the ionosphere and enter outer space. Those waves with frequencies lower than the MUF will partly return to the ground because of reflection and refraction from the ionosphere. The value of the MUF is determined by both the length of the propagation path of the skywave and the state of the ionosphere in the vicinity of the reflection point. The MUF reflects the state of the maximum electron density in a given layer of the ionosphere.

The Optimum Working Frequency (OWF) is the frequency with the highest communication quality in HF skywave communication, as well as the frequency of the highest link establishment probability. In HF communication, it is better to choose a frequency close to the OWF in order to provide a superior effect.

Oblique sounding adopts a two-station cooperative mode of operation in which the transmitting station transmits a radiosonde signal upward diagonally, which will be reflected by the ionosphere and then received by the receiving equipment at a different location, thus obtaining an oblique ionogram. By analyzing the propagation delay of the oblique sounding signal, we are able to calculate the group distance, so as to further obtain the ionospheric information over the relay point of the signal propagation path [14]. In addition, oblique sounding responds to the availability of radio signals of a specific frequency between two locations, and for a given ionospheric channel, only electromagnetic waves of a specific frequency range can be interconnected. The upper limit within this range is the MUF mentioned above, and its lower limit is called the lowest usable frequency (LUF). Therefore, oblique sounding can also be used to carry out the study of the coverage and associated channel characteristics of signals at different frequencies. In this paper, the aim is to validate the frequency selection result based on oblique backscatter sounding.

## 2. Materials and Methods

The frequency selecting method for HF communication based on ionospheric oblique backscatter sounding utilizes a real-time sounding channel, and the main processes are as follows:

First, set up the initial ionospheric background model over the communication link using ionospheric model statistics.

Second, conduct oblique backscatter sounding of the sweep frequency to obtain real ionograms for frequency selection.

Third, separate the echoes in the oblique backscatter ionogram using pattern recognition and extract the parameters from the vertical echo. Invert the ionospheric parameters using the ionospheric inversion method with the created ionospheric background model as the initial value.

Fourth, carry out data fusion using the detection results and inversion results to reconstruct the ionospheric model of the communication link, and then figure out the two-dimensional distribution of electron density with respect to the ground great-circle distance and height in order to describe the ionospheric dynamics of the communication link comprehensively.

Fifth, acquire the usable frequency range of the distance $D$ between the two stations using ray tracing techniques.

Sixth, select the optimal communication frequency based on the energy distribution of the oblique backscatter echo.

Finally, with the help of oblique sounding ionograms, verify that the usable frequency range selected by oblique backscatter sounding has echoes at all of the frequencies on the oblique ionogram, and verify that the selected optimal communication frequency points are close to the OWF.

The flowchart of the algorithm is shown in Figure 1 below.

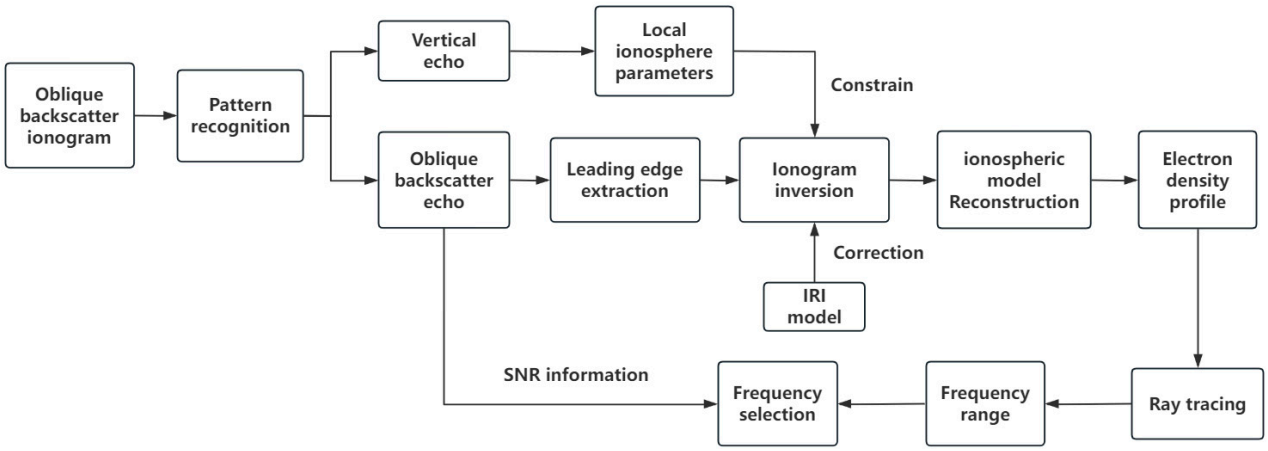



**Figure 1.** Flowchart for frequency selecting method.

Some of the basic methods and algorithms used in this paper are presented in the following sections.

### *2.1. Simulated Ionogram Construction and Pattern Recognition*

While not considering the horizontal inhomogeneity of the ionosphere, the ionospheric monolayer quasi-parabolic (QP) model [15] is commonly used to describe the electron density distribution of the ionosphere. The expression of electron density is as follows:

$$N_e(r) = \begin{cases} N_m\left[1 - \left(\frac{r-r_m}{y_m}\right)^2\left(\frac{r_b}{r}\right)^2\right], r_b < r < r_m\left(\frac{r_b}{r_b - r_m}\right) \\ 0, otherwise \end{cases} \quad (1)$$

$N_e(r)$ represents the electron density of the ionosphere at r kilometers from the Earth's core. As we can see from this expression, electron density is related to a number of factors. $N_m$ indicates the maximum value of electron density in the corresponding ionosphere [16]; in general, $N_m = f_c^2/80.6$ numerically [17]. $f_c$ is the critical frequency derived from ionograms, usually in terms of O mode waves. $r_m$ stands for the height at which the maximum electron density is located, also called the peak height. $r_b$ is the height of the bottom of the ionosphere [18], while $y_m$ stands for half of the thickness of the ionospheric electron density profile and it can be calculated by $y_m = r_m - r_b$.

In the QP model, the relationship between the group path $p'$ of a signal of frequency $f$ and emission elevation $\beta$ and the great-circle distance $D$ can be calculated exactly. According to Croft and Hoogasian [18], the analytical solutions of $p'$ and $D$ are given in Equations (2) and (3).

$$p' = 2\left\{ r_b \sin\gamma - r_0 \sin\beta + \frac{1}{A}\left[ -r_b \sin\gamma - \frac{B}{4\sqrt{A}} \times \ln \frac{\left(B^2 - 4AC\right)}{\left(2Ar_b + B + 2r_b\sqrt{A}\sin\gamma\right)^2} \right] \right\} \quad (2)$$

$$D = 2r_0 \left[ (\gamma - \beta) - \frac{r_0 \cos\beta}{2\sqrt{C}} \ln \frac{B^2 - 4AC}{4C\left(\sin\lambda + \frac{\sqrt{C}}{r_b} + \frac{B}{2\sqrt{C}}\right)^2} \right] \tag{3}$$

We can calculate the parameters in the equations above by using the following method.

$$\begin{cases} A = 1 - \frac{1}{F^2} + \left(\frac{r_b}{F y_m}\right)^2 \\ B = -\frac{2 r_m {r_b}^2}{F^2 {y_m}^2} \\ C = -\left(\frac{r_m r_b}{F y_m}\right)^2 - r_0^2 \cos^2\beta \\ \cos\gamma = \frac{r_0}{r_b}\cos\beta \\ F = \frac{f}{f_c} \end{cases} \tag{4}$$

$\gamma$ is the incident angle of the rays at the bottom of the ionosphere, $r_0$ indicates the radius of the Earth and its value is approximately equal to 6370 km. To determine the ground great-circle distance $D$ in ionospheric oblique sounding, the signal emission elevation angle $\beta$ can be calculated by using the iterative method according to Equation (3). After calculating the value of $\beta$, the group path $p\prime$ will be worked out when $f$ is known if we bring $\gamma$ and $\beta$ into Equation (2).

According to this method, we construct a simulated oblique backscatter ionogram. The ionospheric parameters are obtained based on the IRI model, and IRI is short for International Reference Ionosphere. The IRI model is the model most referenced by current scholars when studying the ionosphere, as well as the most accurate, the most practical, and the most widely used empirical model [19]. The construction of the IRI model relies on a large number of ionospheric sounding systems worldwide and measured data from incoherent scattering radars. Beyond that, it includes part of the Top Ionosphere Sounder survey satellite data. For a certain location, date, and time, the IRI model could serve parameters such as electron density and electron temperature. Furthermore, through the IRI model, we are able to choose the beginning and the end of the height and thus perform the integration to obtain the desired ionospheric parameters. The IRI model is also used in ionogram inversion to make a correction on the result.

By employing the code of the IRI model and inputting the geographic longitude, geographic latitude, altitude range, and time information corresponding to the start and end points of the test link, we are able to obtain the distribution pattern of parameters such as the critical frequency (foF2), peak height (hmF2), and half thickness (ymF2) of the ionosphere F2 layer with different great-circle distances on a link, as well as the distribution of the electron density in the space of the whole link.

In this simulation experiment, we choose the link from Wuhan heading due south, and the great-circle distance of the maximum range is set to 1500 km. We choose the data from 12 October 2023 at a certain time, and the longitude is fixed to that of Wuhan, while the latitude is in 1° steps. The range of the altitude is from 0 to 600 km. Based on these input conditions, we employ the IRI model to obtain ionospheric parameters such as the foF2, ymF2, and hmF2. According to the ionospheric QP model and the equations above [20], an oblique ionogram can be simulated via calculation if the ground great-circle distance $D$ is known [21]. One of the simulated oblique ionograms is shown in Figure 2a, in which the horizontal axis indicates the frequency and the vertical axis indicates the group distance.

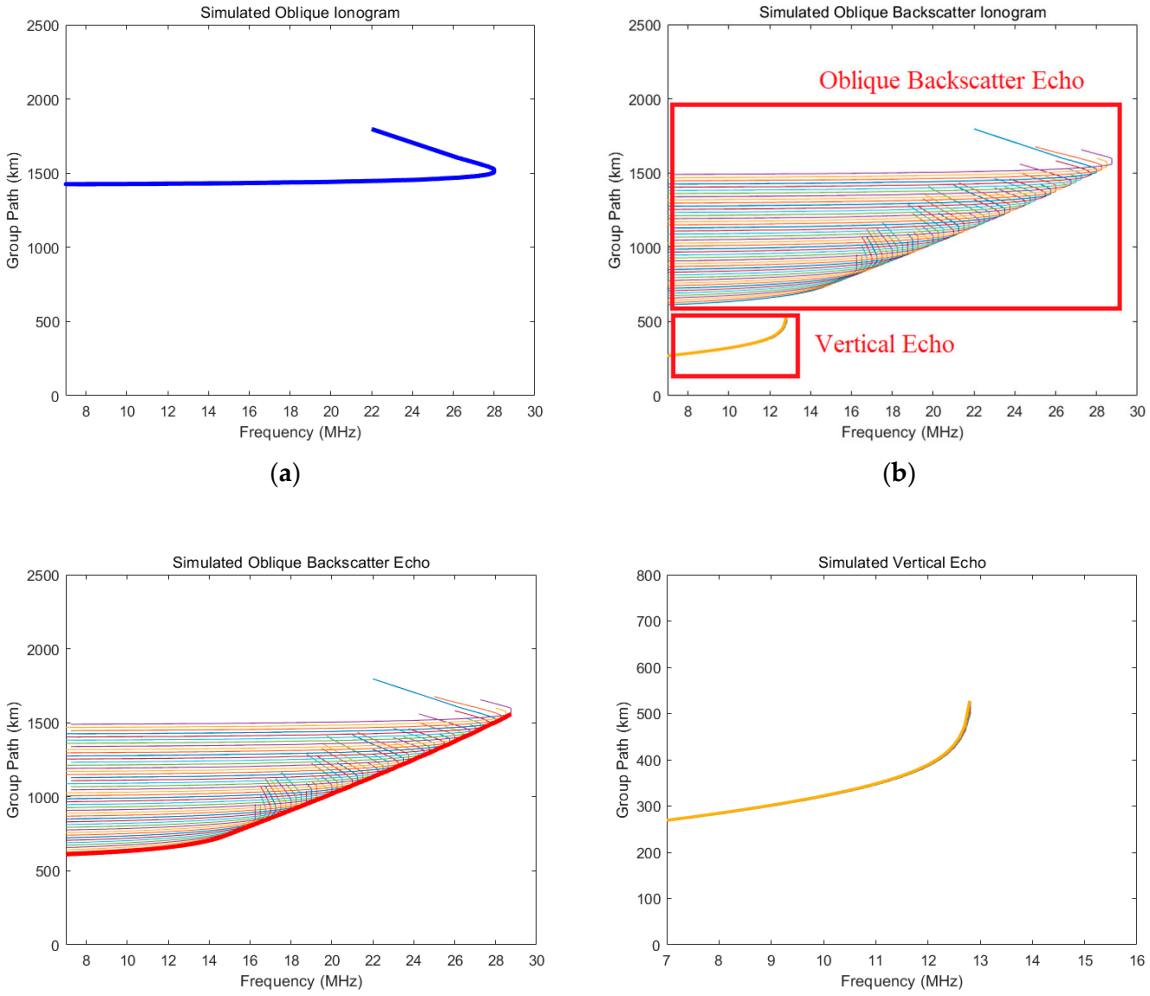



**Figure 2.** (**a**) A simulated oblique ionogram. (**b**) A simulated oblique backscatter ionogram, labeling the oblique backscatter echo and the vertical echo in steps of 0.1 degrees of latitude corresponding to the great-circle distances. The minimum great-circle distance from the starting point is 400 km and the maximum great-circle distance is 1400 km. great-circle distance (**c**) A simulated pure oblique backscatter echo and the leading edge extraction result. (**d**) A simulated pure vertical echo.

After obtaining the oblique ionograms, we superimpose them at different great-circle distances so that we can obtain a simulated oblique backscatter ionogram. As shown in Figure 2b, we can see that the structure of the echo of the simulated oblique backscatter ionogram is similar to that obtained by actual sounding using an ionosonde.

However, due to the wide flap of the transmitting antenna used in oblique backscatter sounding, some of the transmitted signal energy will be emitted in the zenith direction, which makes the ionograms obtained from the detection contain not only the oblique backscatter echo but also the vertical echo, as labeled in Figure 2b. If these two kinds of echo can be separated, the extraction of the leading edge of the oblique backscatter echo is often more accurate. Therefore, we try to pre-process the ionograms and identify the oblique backscatter echo and vertical echo in the oblique backscatter ionograms using the method of pattern recognition. Through the extraction of the vertical echo and the interpretation, we can obtain the information of relevant parameters of the ionosphere and provide a certain reference for the inversion of the oblique backscatter leading edge; through the extraction of the oblique backscatter echo, we can obtain the leading edge of it much more accurately. We use YOLO to perform pattern recognition.

YOLO is one of the deep learning-based algorithms for object detection with advantages of speed and accuracy and is widely used in various fields of computer vision. YOLOv5 is a version of YOLO series, which is a PyTorch -based (version: 1.13.0+cpu) implementation consisting of a backbone network (Backbone), a feature fusion network (Neck), and a prediction network (Head) [22]. When the original image is input into the YOLO network, the backbone network module first extracts features from the image, performs a convolution operation on it, generates three feature maps with different scales after three consecutive down-sampling cycles, and inputs them into the feature fusion module. Then, the Neck module further processes the obtained feature maps and fuses the feature maps at different levels by means of the feature pyramid and path aggregation module, so as to obtain more information about the target. Finally, the fused feature maps are input into the Head module for detection to generate target detection frames, which are labeled with classification information, coordinates, and a confidence level. After the final screening, the overlapping detection frames are merged to obtain the detection results [23]. This method can carry out the function of recognizing and separating the vertical echo and oblique backscatter echo in the ionogram.

We set two types of labels, vertical and backscatter, corresponding to the vertical echo and the oblique backscatter echo, respectively, with the help of the software named LabelImg (version: 1.8.1). LabelImg is a free and open-source tool for graphically labeling an image and creates an XML file or txt file for each image. We label the vertical echo and oblique backscatter echo regions in the ionogram and save the format as .txt file. After these steps, we complete data annotation in yolo label format. We create 350 ionograms as the dataset; in the next step, 80 percent of them are selected as the training dataset and 20 percent are selected as the testing dataset. The number of training rounds is set to 500.

After the training step is completed, the best trained weights are passed into the inference function in the detection function. Finally, we set the path of the image that needs to be subjected to target detection, and then we start pattern recognition and separation at the same time.

Figure 2c,d present a schematic of the separation of the oblique backscatter ionogram, where the vertical echo and the oblique backscatter echo are separated from each other. Next, by finding the minimum value of the group distance corresponding to each frequency point, we can extract the leading edge of the oblique backscatter echo. The red line in Figure 2c shows the simulated extraction of the leading edge.

### *2.2. Ionogram Inversion and Two-Dimensional Electron Density Profile Construction*

Ionogram inversion refers to the derivation of information about the parameters of the ionosphere based on the leading edge of the ionogram echoes. The first step is to set the range of the ionospheric parameters, including the foF2, ymF2, and hmF2. Then, we calculate the leading edge of the oblique backscatter echo under different parameters within the given range of these ionospheric parameters, setting each one up within a group. Next, we compare each leading edge in the group with the measured leading edge extracted from the actual sounding ionogram, using various optimization algorithms to find out the parameter set that produces the best inversion results within the parameter range. Finally, we can obtain the most matching leading edge and the best ionospheric parameters. The ionospheric parameters at this time are believed to be the best ones within the search scope where the best inversion results can be achieved.

The inversion accuracy is strongly correlated with the input of the model parameters. If the range interval of the parameters is found skillfully while setting the model parameters, it is much more likely to achieve the best optimization effect, and the accuracy of the inversion will be greatly improved.

Since the wave elevation angle $\beta$ is a key parameter in calculating $p\prime$ and $D$, it is necessary to figure out $\beta$ first.

When the wave elevation angle $\beta$ is uniquely determined by the calculation in Equation (5), the group path corresponding to the calculation of $\beta$ is the minimum value of the current wave detection frequency, which is the minimum group delay.

By continuously varying the elevation angle $\beta$, all theoretical group path values can be calculated [24]; in this way, the oblique backscatter ionogram traces can be synthesized [25].

$$\cos^2\beta = \left(\frac{r_b}{r_0}\right)^2\left[1-\frac{X^2}{F^2}\left(1+a_1F^2D_0+a_2F^2{D_0}^2+a_3F^4{D_0}^2+a_4F^6{D_0}^3+a_5D_0\right)\right] \quad (5)$$

$r_0$ stands for the radius of the Earth, and some of the parameters are calculated as follows:

$$\begin{cases} D_0 = \frac{y_m}{r_b} \\ X^2 = \frac{r_b^2-r_0^2}{r_b^2-r_0^2+2r_by_m} \\ a_1 = 0.5-X^2 \\ a_2 = 3(X^4-X^6) \\ a_3 = \frac{1-6X^2+10X^4-4X^6}{4(1-X^2)} \\ a_4 = \frac{1-11X^2+44X^4-60X^6+36X^8-8X^{10}}{8(1-X^2)^2} \\ a_5 = 1+X^4 \end{cases} \quad (6)$$

Next, we use the ionospheric inversion algorithm to invert the leading edge of the simulated oblique backscatter ionogram so that we can obtain the distribution of the ionosphere F2 layer parameters such as the foF2, hmF2, and ymF2 with different great-circle distances. In the QP model, it is feasible to work out the electron density at any height once $f_c$, $r_m$, and $r_b$ are known. Hence, a two-dimensional electron density profile based on the inversion result can be constructed.

The background of the image in Figure 3 shows the two-dimensional electron density profile constructed at that moment. The horizontal axis indicates the great-circle distance on the ground, the vertical axis indicates the vertical height from the ground, and the color shades reflect the magnitude of the electron density. The diagram below shows the distribution of electron density at an altitude of 0–600 km within a great-circle distance of 1500 km from Wuhan in a due-south direction.

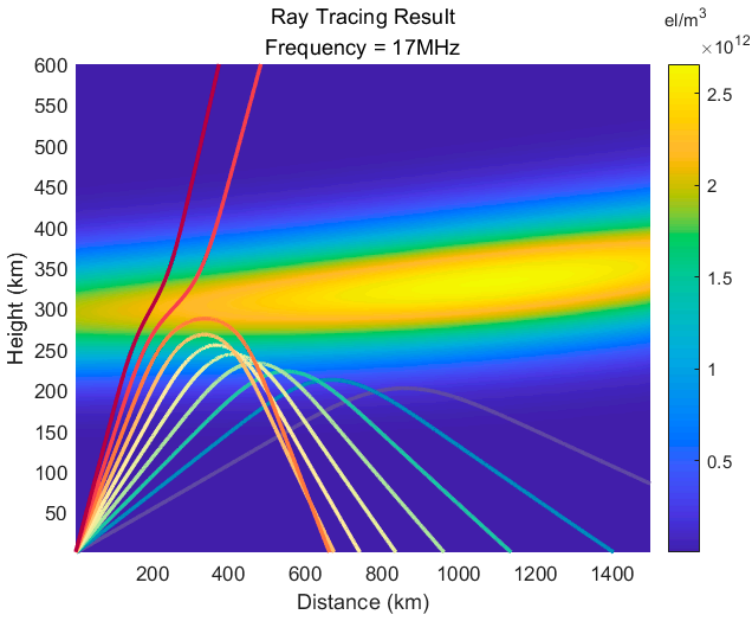



**Figure 3.** A schematic image of the two-dimensional electron density profile and ray tracing result. Rays of different elevation angles are represented by curves of different colors.

### *2.3. Frequency Selection*

The realization of usable frequency range selection utilizes ray tracing techniques. Generally, the problem of HF propagation in the ionosphere can often be solved by using ray tracing methods [26]. It is based on the notion that the wavefield energy of electromagnetic waves propagates approximately along the rays, and the wavefield problem of electromagnetic energy is simplified using optical methods [27]. As a useful tool, ray tracing has a wide range of applications in the fields of radio wave propagation, seismic wave detection, and mobile communication. Ray tracing techniques can be divided into analytic ray tracing techniques and numeric ray tracing techniques [28]. Analytic ray tracing techniques have a clear advantage in terms of speed and computational time, but the specific analytic expressions usually need to be given in the solution, which does not accurately describe the actual ionospheric environment; so, numeric ray tracing techniques are preferred in most cases.

Numeric ray tracing is a method of solving the Haselgrove system of ordinary differential equations [29,30] using numeric methods to obtain the propagation trajectory of radio waves [31]. For electromagnetic waves in the HF band, the variation in ionospheric properties within its wavelength is negligible most of the time, so the propagation of these waves can be approximated by geometrical optics, allowing us to analyze the propagation of radio waves in this band. Numerical ray tracing can graphically describe this matter, and the propagation path of each ray at different frequencies and elevation angles can be seen clearly.

The ray tracing technique can be used to find relationships among ionospheric electron density and signal propagation group paths, ground great-circle distances, elevation, frequency, and so on. Through ray tracing, it is feasible to calculate the usable frequency coverage between two certain places.

Based on this method, the propagation trajectories of rays of different frequencies and elevation angles in this spatial range are calculated, and we record the frequency range $f_1 - f_2$ of the rays that can reach a certain location at a distance $D$ from the starting point. Figure 3 shows the simulation propagation results of the ray whose frequency is 17.0 MHz. We can tell that some of the rays with lower elevation angles are reflected by the ionosphere and end up on the far side of the ground, while some of the rays with higher elevation angles are not able to be reflected by the ionosphere and penetrate out directly. Finally, the usable range is 7.0–18.0 MHz, which is considered the usable frequency range between the starting point and the end point at a specific great-circle distance obtained by employing the IRI model and simulating the construction of the oblique backscatter ionogram. The frequency range of the rays reaching the great-circle distance $D$ is also 7.0–18.0 MHz when the oblique backscatter ionograms are constructed from multiple oblique ionograms in the previous section.

Optimal communication frequency selection is mainly based on the signal-to-noise ratio (SNR) of the oblique backscatter echo. In an ionogram, darker colors indicate a stronger SNR of the echo. Therefore, it is better to choose frequencies with a high SNR at a certain group path value as the optimal selection.

## 3. Experiments and Results Based on Measured Data

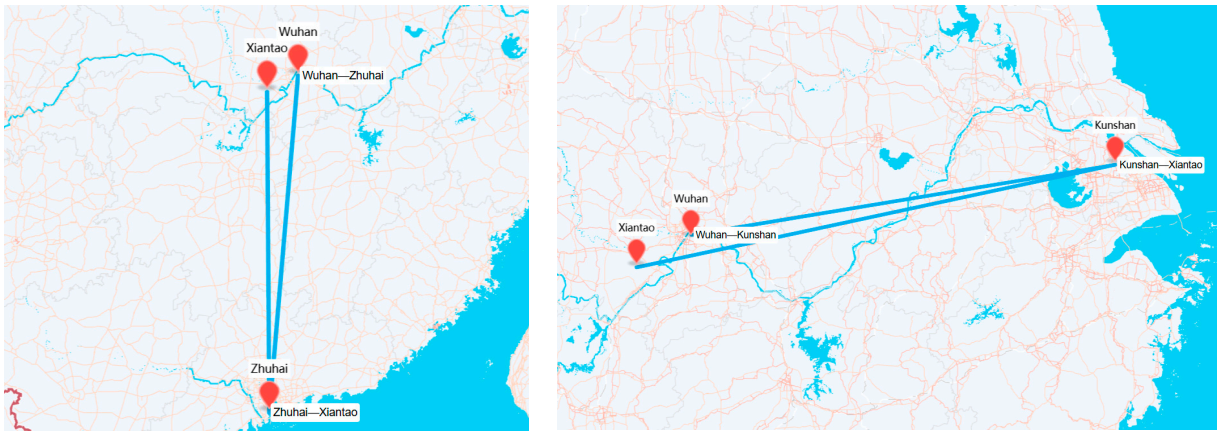
We built two test links to conduct the experiment: one is from Wuhan, Hubei Province, to Zhuhai, Guangdong Province (roughly southward), and the other is from Wuhan, Hubei Province, to Kunshan, Jiangsu Province (roughly eastward). The Wuhan University Ionosphere Laboratory served as the signal transmitting site, transmitting M-sequence-modulated signals through a log-periodic antenna with the use of the Wuhan Ionospheric Sounding System (WISS) [32,33] developed by the Wuhan University Ionosphere Laboratory independently. At the station in Xiantao, Hubei Province, a dipole antenna was set up to receive the oblique backscatter echoes. The specific parameters are shown in Table 1.

**Table 1.** Transmitting and receiving parameters.

| Item | Specification |
|---|---|
| Transmitting Site | log-periodic antenna |
| Receiving Site | dipole antenna |
| Average Transmitting Power | 500 W |
| Code System | m-sequence |
| Code Order | 8 |
| Code Width | 4 |
| Pulse Width | 4 |
| DDC Rate | 39.0625 kHz |
| Detection Period | 484 s |

The geographic coordinates of the Wuhan site are 30.54°N, 114.3°E, while those of the Zhuhai site are 22.35°N, 113.59°E, and the ground great-circle distance between it and the Wuhan site is 915 km. Similarly, the geographic coordinates of the Kunshan site are 31.50°N, 120.95°E, and the ground great-circle distance is calculated to be 635 km.

The distance between the Wuhan and Xiantao stations is relatively small compared with the distance between the Wuhan and Zhuhai and Kunshan stations, which has little influence on frequency selection and can be ignored. The specific station locations and their relative position information are shown in Figure 4 below.




(**a**) (**b**)

**Figure 4.** Two test links: (**a**) Wuhan–Zhuhai link; (**b**) Wuhan–Kunshan link.

### *3.1. Experiment of Wuhan–Zhuhai Link*

First, we take the Wuhan–Zhuhai link as an example. The initial ionospheric background model over the link is established using the IRI model statistical data, followed by ionospheric oblique backscatter sweep sounding to obtain the measured ionogram. The obtained oblique backscatter ionogram is shown in Figure 5a.

It can be seen that the oblique backscatter ionogram includes two regions of echo, the oblique backscatter echo and the vertical echo. We try to separate these two parts using the pattern recognition method in order to obtain the pure oblique backscatter echo and the pure vertical echo.

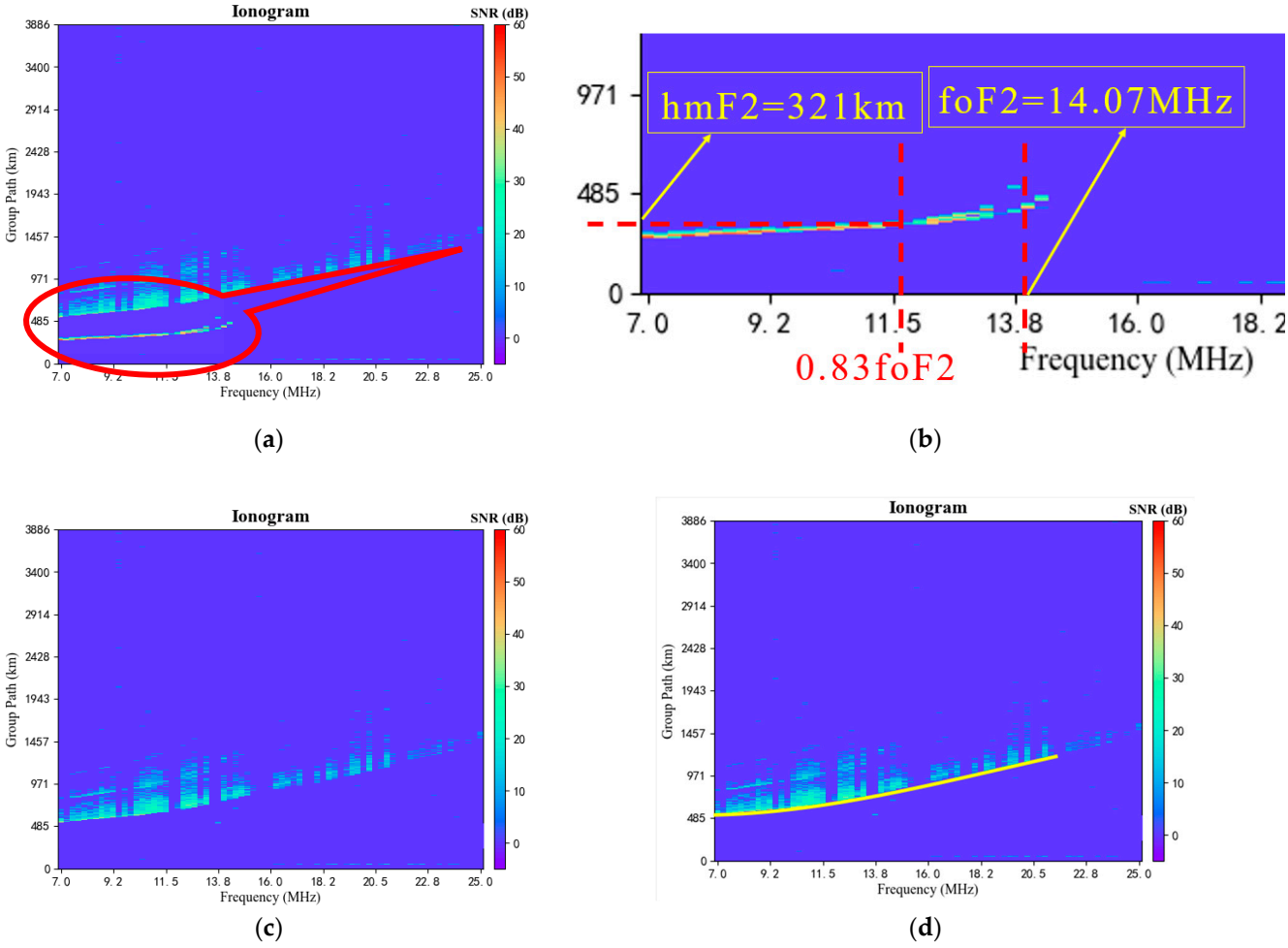



**Figure 5.** (**a**) The oblique backscatter ionogram of the Wuhan–Zhuhai link; (**b**) the vertical echo separated from the ionogram and parameter reading results; (**c**) the oblique backscatter echo separated from the ionogram. (**d**) The result of leading edge extraction of the Wuhan–Zhuhai link ionogram.

We use YOLOv5 for pattern recognition. If the pure vertical echo is separated, we can extract the local ionospheric parameters from it. In this ionogram, the critical frequency of the F2 layer (foF2) is read as 14.07 MHz from the vertical echo. According to the empirical formula for the peak height of the F2 layer in the vertical echo, $hpF2 = h(foF2 \times 0.83)$ [34]. The symbol $h$ in the equation stands for the virtual height of the vertical echo with a certain frequency. Since the difference between hmF2 and hpF2 is usually not very large, we can obtain the value of the hmF2, which is approximately equal to 321 km. These two parameters will be helpful in the inversion of the ionograms.

Next, we extract the leading edge of the oblique backscatter echo, as shown in Figure 5d. From the leading edge, it can be seen that the frequency corresponding to the end point of the leading edge is about 21 MHz, and we can further figure out the maximum group distance, which is about 1200 km. Due to multiple factors such as the condition of the ionosphere, the property of the sounding systems, and the characteristics of wave propagation, it is not realistic to obtain the echoes at a frequency more than 21 MHz; so, the intensity of the oblique backscatter echo is weak at higher frequencies. In line with the characteristics of the oblique backscatter inversion, assuming that the maximum group distance can reach the value of 1200 km, only the ionospheric parameters within around 600 km can be estimated. In this condition, we try to extend the oblique backscatter leading edge in line with its changing rule to obtain the ionospheric parameters over regions greater than 600 km.

Based on the changing rule of the oblique backscatter leading edge, we try three types of curve fitting: exponential function fitting, cubic polynomial fitting, and linear fitting. Figure 6 shows the results of extending the oblique backscatter leading edge, where the curve is extended to a frequency of 35.0 MHz. The thick red curve shows the original oblique backscatter leading edge, and the blue curve shows a cubic polynomial fitting result for the curve, with the expression being $y = ax^3 + bx^2 + cx + d$. The green curve shows an exponential fitting result for the curve and the expression is $y = ae^{bx} + ce^{dx}$. The orange curve shows the result of linear fitting, whose expression is $y = ax + b$. After fitting with each of the three methods, we calculate whether the fitted curves are consistently incremental over the frequency range, in which case the curve needs to be in line with the trend of the leading edge. If these curves all satisfy the conditions, we further compute their adjusted R-square and relative root mean squared error (RMSE), make a quantitative comparison, and then select the better fitting method.

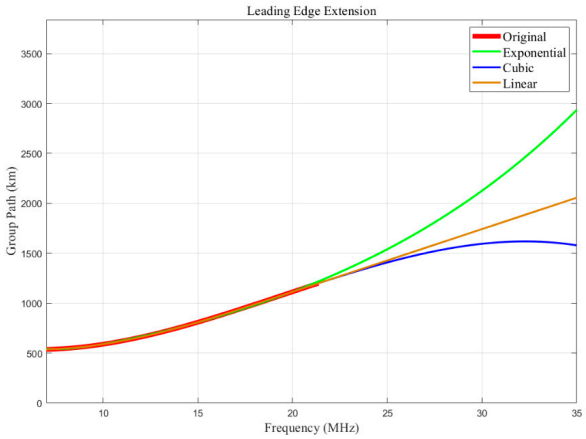



**Figure 6.** An extension of the extracted oblique backscatter leading edge.

The RMSE and the adjusted R-squared value are calculated by using the following formulas:

$$RMSE = \sqrt{\frac{1}{n}\sum_{i}^{n}(y_i - \hat{y}_i)^2} \tag{7}$$

$$R^2 = 1 - \frac{\sum_{i}^{n}(y_i - \hat{y}_i)^2}{\sum_{i}^{n}(y_i - \overline{y}_i)^2} \tag{8}$$

$$R^2(adj) = 1 - \frac{(1 - R^2)(n - 1)}{n - p - 1} \tag{9}$$

$y_i - \hat{y}_i$ indicates the difference between the true value and the fitted value, while $y_i - \overline{y}_i$ indicates the difference between the true value and the mean value; n denotes the number of samples, and p is the number of variables. The larger $R^2(adj)$ is, the better the fitting effect.

In this example, it can be seen from the trend of the curves in the figure that the trend of the cubic polynomial fitting curve does not correspond to the trend of the ionospheric leading edge, and we choose the exponential fitting curve after comparing the adjusted R-squared values. The value is 0.9951, which can better reflect the trend of the leading edge. By extending the curve to a frequency value of about 35.0 MHz, in this way, the group distance will also be extended to more than 2000 km.

We take advantage of ionospheric inversion techniques to invert the extended leading edge in order to obtain the relationship of the critical frequency, peak height, and half thickness of the F2 layer in the refractive zone with the great-circle distance, as well as to

construct a two-dimensional electron density profile for describing the ionospheric posture in the refractive zone.

Hereafter, we utilize the ray tracing technique to calculate the usable frequency coverage between Wuhan and Zhuhai. The search frequency of the rays starts from 7.0 MHz and ends at 25.0 MHz with a step of 0.5 MHz, and the rays are searched at elevation angles ranging from 15° to 60° with a step of 5°. Figure 7 shows the ray tracing results for different frequencies; the specific values of the four figures are 8.0 MHz, 14.5 MHz, 17.5 MHz, and 19.0 MHz. The background of the image shows the two-dimensional electron density profile constructed at that moment. The horizontal axis indicates the great-circle distance from the Wuhan station, the vertical axis indicates the vertical height from the ground, and the gradation of color reflects the electron density. In Figure 7a, the rays simulate the propagation trajectories of radio waves at 17.5 MHz but with different elevation angles, indicated by different colors. It can be seen from the four figures that there is always at least one ray that reaches the specified ground distance in each figure, proving that these frequencies of the rays are usable.

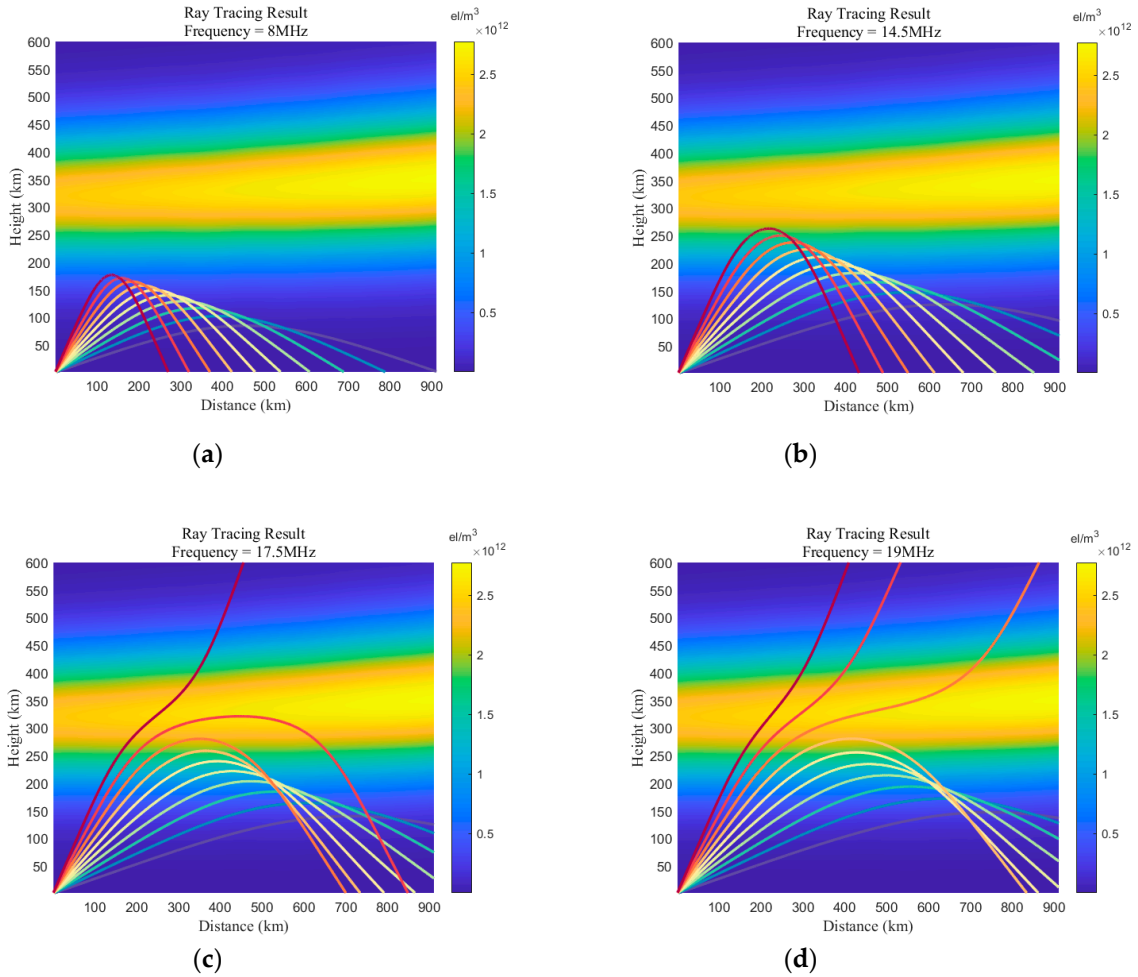



**Figure 7.** The two-dimensional electron density profile and ray tracing result of different frequencies of the Wuhan–Zhuhai link. Rays of different elevation angles are represented by curves of different colors. (**a**) The ray with a frequency of 8.0 MHz; (**b**) the ray with a frequency of 14.5 MHz; (**c**) the ray with a frequency of 17.5 MHz; (**d**) the ray with a frequency of 19.0 MHz.

As a result, the usable frequency range is 8.0–19.0 MHz for the required communication distance of 915 km.

Based on the correspondence between the group distance and the great-circle distance after the oblique backscatter inversion, the P-D transformation relation is derived [35]. In

the ionospheric monolayer QP model, we can obtain the relationship between the group distance $P$ of a ray with frequency $f$ and elevation $\beta$ and the ground great-circle distance $D$ between the ray receiving point and the transmitting point directly via ionogram inversion. After the inversion, we can obtain the plot of the correspondence between $P$ and $D$, as shown in Figure 8.

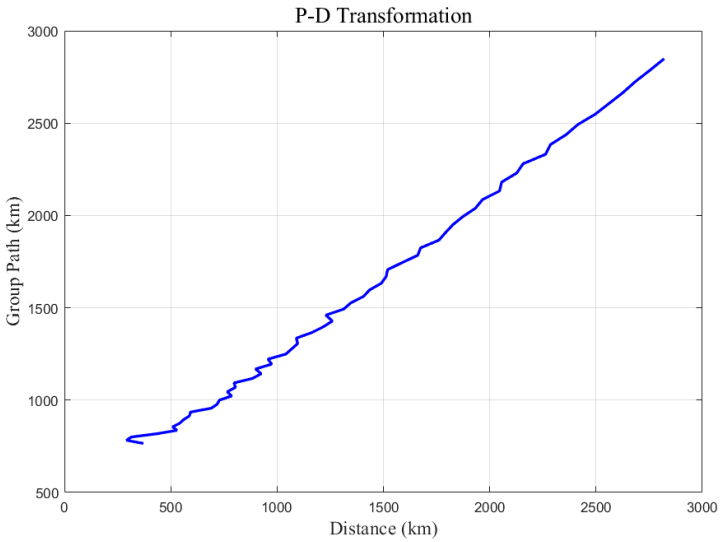



**Figure 8.** The plot of the P-D transformation of the Wuhan–Zhuhai link.

According to the required communication distance $D = 915$km, we can derive the corresponding group distance $P = 1163$km. Based on the energy distribution of the oblique backscatter echo, we can select the optimal communication frequency and the corresponding SNR within the usable frequency range and in areas larger than the critical frequency obtained by the vertical echo. From this ionogram, the three frequencies corresponding to the best SNR are 17.0 MHz, 16.5 MHz, and 16.2 MHz. The specific frequencies corresponding to the best SNR are shown in Table 2 below, and these three frequencies are taken as the selected better HF communication frequencies.

**Table 2.** Frequency selection result and SNR of Wuhan–Zhuhai link.

| Frequency (MHz) | SNR (dB) |
|---|---|
| 17.0 | 7.0 |
| 16.5 | 5.9 |
| 16.2 | 5.8 |

At the same time, we set up a two-wire antenna to receive ionospheric oblique sounding echoes at the Zhuhai site. The maximum usable frequency can be read out from the oblique ionogram obtained at the same moment (shown in Figure 9b), and the value is about 19.0 MHz. It can be seen that there are oblique echoes in the frequency range from 8.0 MHz to 19.0 MHz, which proves that the frequency range selected from the oblique backscatter ionogram is feasible for communication.

The MUF acquired from ray tracing is 19.0 MHz, and according to the relation $OWF = 0.85 \times MUF$, the OWF is around 16.2 MHz; the frequency points selected in the oblique backscatter ionogram are close to it. It is considered that these three frequency points are the optimal communication frequencies between Wuhan and Zhuhai under the current ionospheric condition.

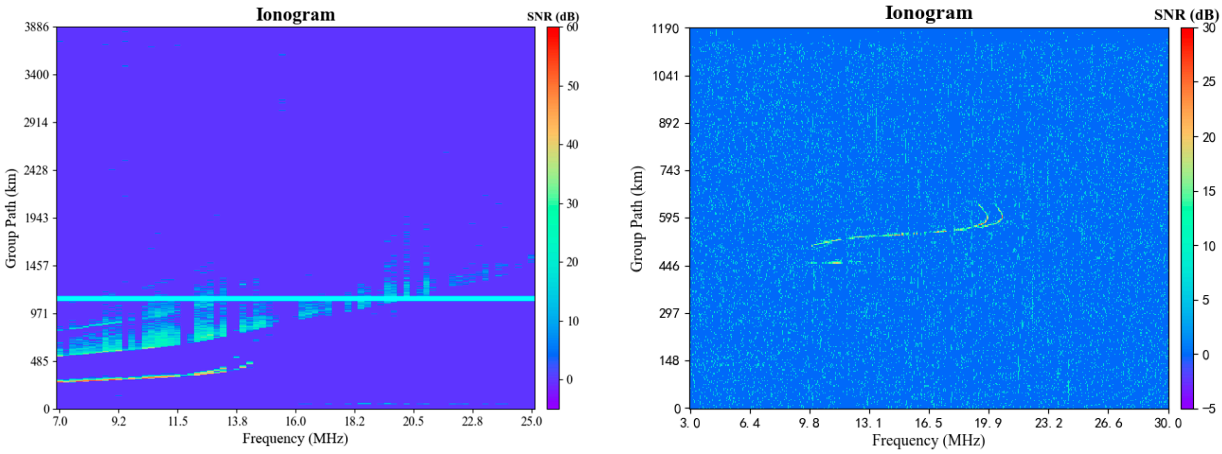



**Figure 9.** (**a**) The oblique backscatter ionogram for frequency selection; the blue line indicates the group path value; (**b**) the oblique ionogram received at the same time by the ionosonde at Zhuhai.

### *3.2. Experiment of Wuhan–Kunshan Link*

Then, we carry out the experiment for the other link, Wuhan–Kunshan, for frequency selection in the same way as for the Wuhan–Zhuhai link above. The obtained oblique backscatter ionogram is shown in Figure 10a.

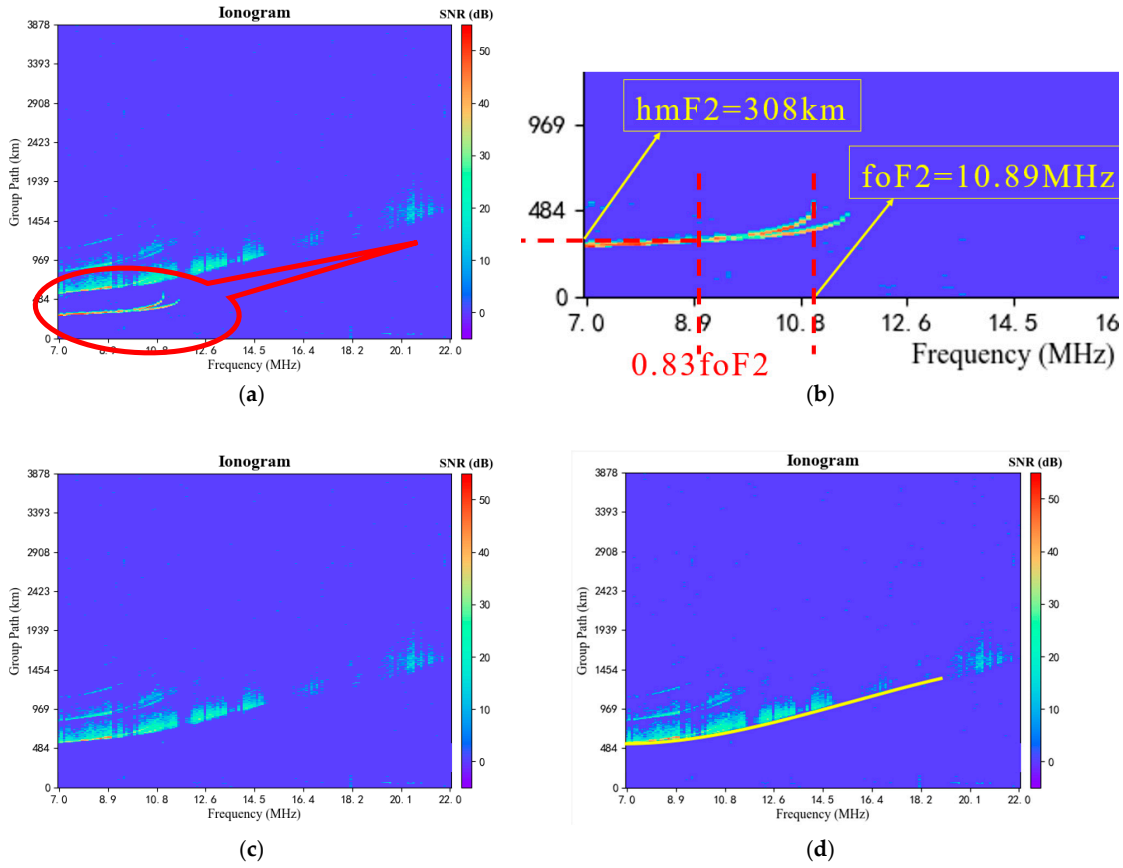



**Figure 10.** (**a**) The oblique backscatter ionogram of the Wuhan–Kunshan link. (**b**) The vertical echo separated from the ionogram and the parameter reading results. (**c**) The oblique backscatter echo separated from the ionogram. (**d**) The result of leading edge extraction of the Wuhan–Kunshan link ionogram.

The two parts of the echoes are separated using the pattern recognition method. Then, from the vertical echo, the local critical frequency of the local F2 layer is read as 10.89 MHz and the peak height of the F2 layer is approximately 308 km.

Next, we extract the leading edge of the oblique backscatter echo and conduct an inversion to obtain the relationship of the critical frequency, peak height, and half thickness of the F2 layer in the refractive zone with the great-circle distance. The next step is to create a two-dimensional electron density profile. Then, we calculate the usable frequency coverage between Wuhan and Kunshan. The range of the search frequency and the elevation range of the rays are the same as those of the Wuhan–Zhuhai link. Figure 11 shows the two-dimensional electron density profile and the ray tracing results for different frequency values of 7.0 MHz, 9.5 MHz, 11.5 MHz, and 13.5 MHz. Finally, we obtain the usable frequency range between Wuhan and Kunshan on this link as 7.0–13.5 MHz.

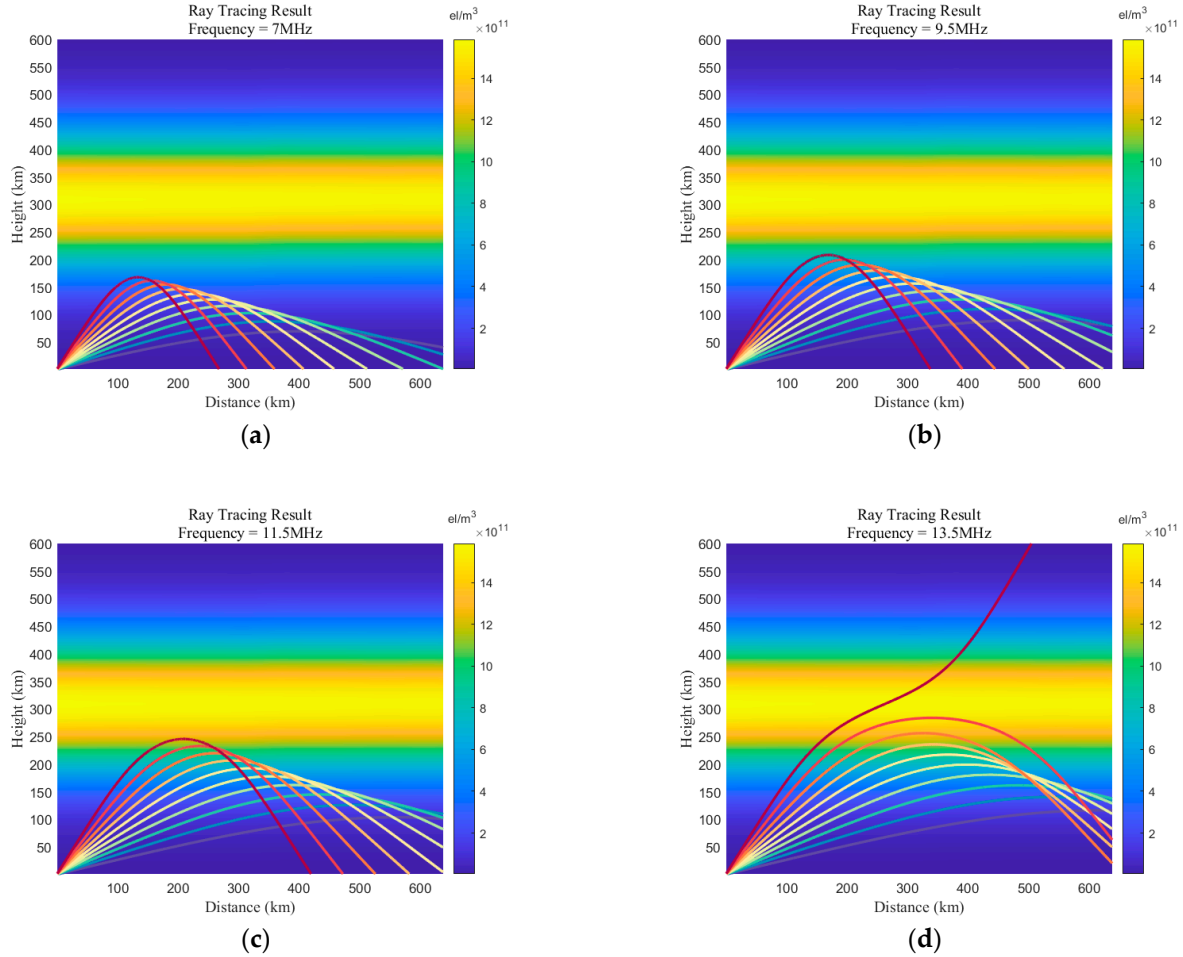



**Figure 11.** The two-dimensional electron density profile and ray tracing result of different frequencies of the Wuhan–Kunshan link. Rays of different elevation angles are represented by curves of different colors. (**a**) The ray with a frequency of 7.0 MHz; (**b**) the ray with a frequency of 9.5 MHz; (**c**) the ray with a frequency of 11.5 MHz; (**d**) the ray with a frequency of 13.5 MHz.

Similarly, the relationship between the group path $P$ and the great-circle distance $D$ can be reflected in the diagram in Figure 12.

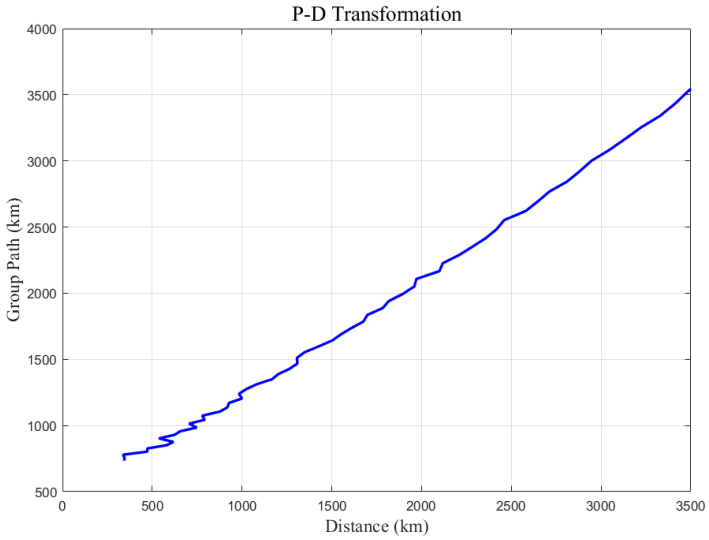


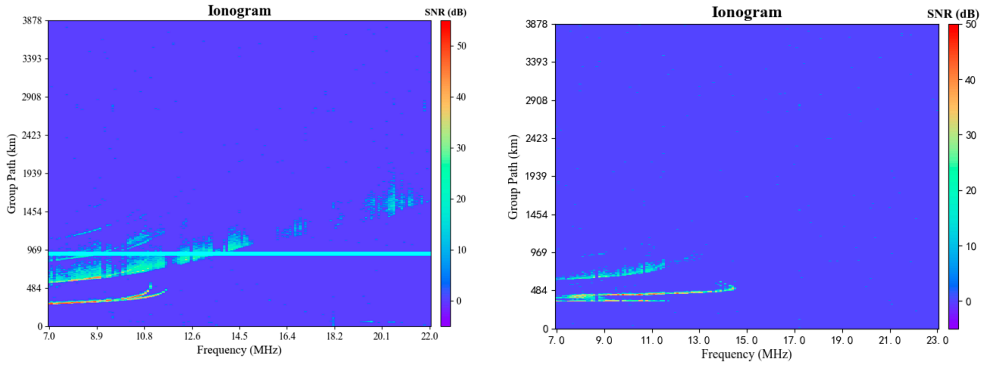

**Figure 12.** The plot of the P-D transformation of the Wuhan–Kunshan link.

According to the required communication distance $D = 635$km, we can derive the corresponding group distance $P = 927$km. Using the same method, we can ascertain that the five frequencies corresponding to the best SNR are 12.8 MHz, 13.1 MHz, 12.5 MHz, 12.7 MHz, and 12.3 MHz. The specific frequencies corresponding to the best SNR are shown in Table 3. These five frequencies are taken as the selected better HF communication frequencies.

**Table 3.** Frequency selection result and SNR of Wuhan–Kunshan link.

| Frequency (MHz) | SNR (dB) |
|---|---|
| 12.8 | 25.0 |
| 13.1 | 23.8 |
| 12.5 | 23.0 |
| 12.7 | 22.7 |
| 12.3 | 22.1 |

Similarly, we set up a two-wire antenna to receive ionospheric oblique sounding echoes at the Kunshan site. The MUF read from the oblique ionogram (shown in Figure 13b) is about 14.2 MHz. It can be seen that there are oblique echoes in the frequency range from 7.0 MHz to 13.5 MHz, proving that the frequency range selected from the oblique backscatter ionogram is feasible for communication.




(**a**) (**b**)

**Figure 13.** (**a**) The oblique backscatter ionogram for frequency selection; the blue line indicates the group path value. (**b**) The oblique ionogram received at the same time by the ionosonde at Kunshan.

The MUF acquired from ray tracing is 14.0 MHz. Then, we ascertain that the OWF is around 11.9 MHz, so the frequency points selected in the oblique backscatter ionogram are close to it. It is considered that these five frequency points are the optimal communication frequencies between Wuhan and Kunshan under the current ionospheric condition.

### *3.3. Comparison of MUF Obtained from Oblique Backscatter Ray Tracing and Oblique Sounding*

A total of 126 sounding data points from the Kunshan and Zhuhai stations were accumulated to compare the MUF obtained from the oblique backscatter ionograms and the MUF read from the oblique ionograms obtained from the soundings at the corresponding moments. The variation is shown in Figure 14.

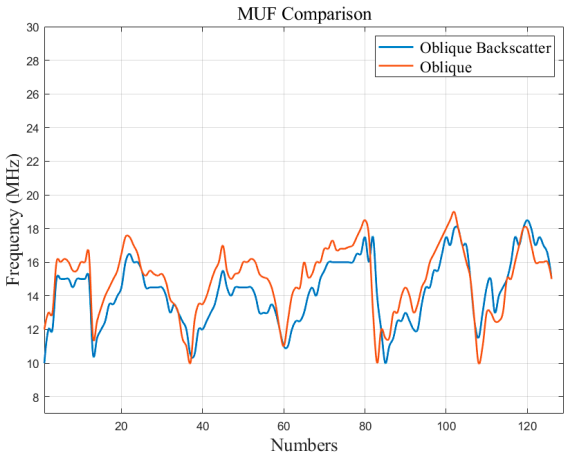



**Figure 14.** The result of the comparison of the MUF obtained from oblique backscatter ray tracing and oblique sounding. The blue line refers to the statistical MUF data obtained from the oblique backscatter ionograms, while the red line refers to the statistical MUF data read from the oblique ionograms.

Based on the formulas of the Mean Absolute Percentage Error (MAPE) and RMSE below [36], the MAPE of the MUF selected in the oblique backscatter ionograms and the MUF read from the oblique ionograms at the corresponding moment is 7.8%, while the RMSE is 1.34 MHz.

$$MAPE = \frac{100\%}{n}\sum_{i=1}^{n}\left|\frac{y_{i,Oblique} - y_{i,Backscatter}}{y_{i,Oblique}}\right| \tag{10}$$

$$RMSE = \sqrt{\frac{1}{n}\sum_{i}^{n}\left(y_{i,Oblique} - y_{i,Backscatter}\right)^2} \tag{11}$$

## 4. Conclusions

In this paper, a frequency selecting method for HF communication based on ionospheric oblique backscatter sounding is designed which utilizes ionospheric sounding, pattern recognition, ionogram inversion, ray tracing, and other techniques to select the usable frequency range under the current situation, as well as identifying the best communication frequency points through the processing of the oblique backscatter ionograms. After verification, the selected frequency range has echoes distributed in the corresponding detected oblique ionogram, and the selected frequency points have a single mode which better reduces the influence of multipath effects and consequently has better communication effects.

For future research, the proposed method can be improved in three main directions. The first is to improve the accuracy of ionogram inversion, so that the inversion of ionospheric parameters and the construction of electron density profiles can be more precise; thus, the frequency selection results will be much more reliable. The second is to accumulate real-time ionospheric sounding data and to build a machine learning model by

combining historical ionospheric sounding data, frequency data, and environmental monitoring data, so as to realize the prediction and recommendation of the available frequencies with different temporal and spatial granularity degrees. The third is to incorporate some other factors into the present method, such as the Es layer and ionospheric disturbances, to make the frequency selection method more applicable and accurate.

**Author Contributions:** Conceptualization, C.C. and G.Y.; methodology, T.L.; software, C.J.; validation, C.C.; investigation, G.Y.; data curation, C.C., G.Y. and T.L.; writing—original draft preparation, C.C.; writing—review and editing, C.C. and G.Y.; visualization, C.C. and C.J.; project administration, G.Y. and T.L.; funding acquisition, T.L. and C.J. All authors have read and agreed to the published version of the manuscript.

**Funding:** This research was funded by the National Natural Science Foundation of China (42104151/42074184) and the National Key Research and Development Program of China (2023YFA1009100).

**Data Availability Statement:** The data are available from Guobin Yang upon request (gbyang@whu.edu.cn) due to. . .scientific research and cooperation.

**Conflicts of Interest:** The authors declare no conflicts of interest.

## References

1. Wang, J.; Shi, Y.; Yang, C.; Zhang, Z.; Zhao, L. A Short-Term Forecast Method of Maximum Usable Frequency for HF Communication. *IEEE Trans. Antennas Propag.* **2023**, *71*, 5189–5198. [CrossRef]
2. Wang, J.; Shi, Y.; Yang, C.; Feng, F. A review and prospects of operational frequency selecting techniques for HF radio communication. *Adv. Space Res.* **2022**, *69*, 2989–2999. [CrossRef]
3. Wang, J.L.; Ding, G.R.; Wang, H.C. HF Communications: Past, Present, and Future. *China Commun.* **2018**, *15*, 1–9. [CrossRef]
4. Burr, A.G. Application of space-time coding techniques in third generation systems. In Proceedings of the 1st International Conference 3G Mobile Communication Technologies, London, UK, 27–29 March 2000; pp. 276–280.
5. Albertson, R.; Arthur, J.; Rashid, M.H. Overview of electromagnetic interference. In Proceedings of the 38th Annual North American Power Symposium (NAPS), So Illinois Univ Carbondale, Carbondale, IL, USA, 17–19 September 2006; pp. 263–266.
6. Hanasaki, N.; Kagoshima, S.; Miura, N.; Saito, G. Pressure effects to the anomalous state of quasi two-dimensional conductor $\alpha$-(BEDT-TTF)$_2$KHg(SCN)$_4$. *J. Phys. Soc. Jpn.* **1996**, *65*, 1010–1018. [CrossRef]
7. Uryadov, V.P.; Vybornov, F.I.; Kolchev, A.A.; Vertogradov, G.G.; Sklyarevsky, M.S.; Egoshin, I.A.; Shumaev, V.V.; Chernov, A.G. Impact of heliogeophysical disturbances on ionospheric HF channels. *Adv. Space Res.* **2018**, *61*, 1837–1849. [CrossRef]
8. Hirose, M.; Imai, T.; Wu, S.; Iwasaki, S.; Ching, G.S.; Kishiki, Y. A Ray Tracing Parameter Optimization System in Mobile Radio Propagation Prediction. In Proceedings of the 2022 International Workshop on Antenna Technology (iWAT), Dublin, Ireland, 16–18 May 2022; pp. 269–270.
9. Liu, T.; Yang, G.; Zhao, Z.; Jiang, C.; Hu, Y. Application of Beamforming Technology in Ionospheric Oblique Backscatter Sounding with a Miniaturized L-Array. *Remote Sens.* **2020**, *12*, 499. [CrossRef]
10. Li, Z.L.; Peng, H.; Zuo, Y.L.; Su, J.X.; Yang, S.H. The focusing effect in backward Raman amplification in plasma. *Phys. Plasmas* **2018**, *25*, 043109. [CrossRef]
11. Zhao, J.J.; Zhou, C.; Yang, G.B.; Jiang, C.H.; Chang, S.S.; Zhu, P.; Gu, X.D.; Ni, B.B.; Zhao, Z.Y. A new inversion algorithm for backscatter ionogram and its experimental validation. *Ann. Geophys.* **2014**, *32*, 465–472. [CrossRef]
12. Wang, J.; Han, H.; Shi, Y.; Yang, C.; Liu, Y.; Wang, Z. Comparison and validation of MOF observations and MUF predictions from seven different models. *Adv. Space Res.* **2024**, *74*, 2452–2462. [CrossRef]
13. Mahmoud, S.F.; Antar, Y.M.M. High Frequency Ground Wave Propagation. *IEEE Trans. Antennas Propag.* **2014**, *62*, 5841–5846. [CrossRef]
14. Sergeeva, M.A.; Gonzalez-Esparza, J.A.; Blagoveshchensky, D.V.; Maltseva, O.A.; Chernov, A.G.; Corona-Romero, P.; De la Luz, V.; Mejia-Ambriz, J.C.; Gonzalez, L.X.; Romero-Hernandez, E.; et al. First observations of oblique ionospheric sounding chirp signal in Mexico. *Results Phys.* **2019**, *12*, 1002–1003. [CrossRef]
15. Norman, R.J. Backscatter ionogram inversion. In Proceedings of the International Conference on Radar, Adelaide, Australia, 3–5 September 2003; pp. 368–374.
16. Ponomarchuk, S.N.; Penzin, M.S. The inversion of backscatter ionograms by continuous chirp signal. In Proceedings of the 25th International Symposium On Atmospheric and Ocean Optics—Atmospheric Physics, Novosibirsk, Russia, 30 June–5 July 2019.
17. Ponomarchuk, S.N.; Penzin, M.S. Inversion of backscatter ionograms into quasiparabolic ionospheric layer parameters. *Sol. -Terr. Phys.* **2020**, *6*, 5.
18. Croft, T.A.; Hoogasian, H. Exact ray calculations in a quasi-parabolic ionosphere with no magnetic field. *Radio Sci.* **1968**, *3*, 69–74. [CrossRef]
19. Bilitza, D. International Reference Ionosphere 2000. *Radio Sci.* **2001**, *36*, 261–275. [CrossRef]

20. Benito, E.; Bourdillon, A.; Saillant, S.; Rannou, V.; Molinié, J.P. Inversion of HF backscatter ionograms using elevation scans. *J. Atmos. Sol. -Terr. Phys.* 2008; 70, 1935–1948. [CrossRef]
21. Song, H.; Hu, Y.; Jiang, C.; Zhou, C.; Zhao, Z. Automatic scaling of HF swept-frequency backscatter ionograms. *Radio Sci.* **2015**, *50*, 381–392. [CrossRef]
22. Redmon, J.; Divvala, S.; Girshick, R.; Farhadi, A. You Only Look Once: Unified, Real-Time Object Detection. In Proceedings of the 2016 IEEE Conference on Computer Vision and Pattern Recognition (CVPR), Las Vegas, NV, USA, 27–30 June 2016; pp. 779–788.
23. Yan, F.; Xu, Y. Improved Target Detection Algorithm Based on YOLO. In Proceedings of the 2021 4th International Conference on Robotics, Control and Automation Engineering (RCAE), Wuhan, China, 4–6 November 2021; pp. 21–25.
24. Huang, X.; Li, Y. Determining the ground range using the HF backscatter ionogram leading edge. *Chin. J. Radio Sci.* **1986**, *1*, 36–42.
25. Song, J.; Zhao, Z.Y.; Zhou, C.; Chen, G. Inversion of HF sweep-frequency backscatter ionograms. *Chin. J. Geophys. Chin. Ed.* **2011**, *54*, 1953–1959.
26. Erdem, E.; Arikan, F. Ray Tracing on Stratified Plane Ionosphere Model. In Proceedings of the 22nd IEEE Signal Processing and Communications Applications Conference (SIU), Karadeniz Teknik Univ, Trabzon, Turkey, 23–25 April 2014; pp. 1391–1394.
27. Cacciamano, A.; Capria, A.; Berizzi, F.; Martorella, M.; Mese, E.D. A ray tracing based method for coarse coordinate registration in HF skywave OTH radar. In Proceedings of the 6th European Radar Conference, Rome, Italy, 30 September–2 October 2009; pp. 204–207.
28. Zhu, P.; Zhou, C.; Zhang, Y.; Yang, G.; Jiang, C.; Sun, H.; Cui, X. F region electron density profile inversion from backscatter ionogram based on international reference ionosphere. *J. Atmos. Sol. Terr. Phys.* **2015**, *129*, 111–118. [CrossRef]
29. Azzarone, A.; Bianchi, C.; Pezzopane, M.; Pietrella, M.; Scotto, C.; Settimi, A. IONORT: A Windows software tool to calculate the HF ray tracing in the ionosphere. *Comput. Geosci.* **2012**, *42*, 57–63. [CrossRef]
30. Pederick, L.H.; Cervera, M.A.; Harris, T.J. Interpreting Observations of Large-Scale Traveling Ionospheric Disturbances by Ionospheric Sounders. *J. Geophys. Res. Space Phys.* **2017**, *122*, 12556–12569. [CrossRef]
31. Cervera, M.A.; Harris, T.J. Modeling ionospheric disturbance features in quasi-vertically incident ionograms using 3-D magnetoionic ray tracing and atmospheric gravity waves. *J. Geophys. Res. Space Phys.* **2014**, *119*, 431–440. [CrossRef]
32. Chen, G.; Zhao, Z.Y.; Zhang, Y.N. Ionospheric Doppler and echo phase measured by the Wuhan Ionospheric Oblique Backscattering Sounding System. *Radio Sci.* **2007**, *42*, 1–13. [CrossRef]
33. Chen, G.; Zhao, Z.Y.; Yang, G.B.; Zhou, C.; Yao, M.; Li, T.; Huang, S.; Li, N. Enhancement and HF Doppler observations of sporadic-E during the solar eclipse of 22 July 2009. *J. Geophys. Res. Space Phys.* **2010**, *115*, 1–11. [CrossRef]
34. Pillat, V.G.; Guimarães, L.N.F.; Fagundes, P.R.; da Silva, J.D.S. A computational tool for ionosonde CADI's ionogram analysis. *Comput. Geosci.* **2013**, *52*, 372–378. [CrossRef]
35. Dyson, P.L.; Bennett, J.A. Exact Ray Path Calculations Using Realistic Ionospheres. *Iee Proc. H Microw. Antennas Propag.* **1992**, *139*, 407–413. [CrossRef]
36. Chicco, D.; Warrens, M.J.; Jurman, G. The coefficient of determination R-squared is more informative than SMAPE, MAE, MAPE, MSE and RMSE in regression analysis evaluation. *PeerJ Comput. Sci.* **2021**, *7*, e623. [CrossRef]


**Disclaimer/Publisher's Note:** The statements, opinions and data contained in all publications are solely those of the individual author(s) and contributor(s) and not of MDPI and/or the editor(s). MDPI and/or the editor(s) disclaim responsibility for any injury to people or property resulting from any ideas, methods, instructions or products referred to in the content.